POSITION SENSITIVE IONIZATION CHAMBER

Sh. Zeynalov[1)], O. Zeynalova[1)], F.-J. Hambsch[2)], P. Sedyshev[1)],
V. Shvetsov[1)], V. Smirnov[1)]

1) Joint Institute for Nuclear Research, Joliot-Curie 6, 141980 Dubna, Moscow region, Russia
2) European Commission, Joint Research Centre, Institute for Reference Materials and Measurements, Retieseweg 111, 2440 Geel, Belgium

Abstract. In this work we report recent achievements in design of twin back-to-back ionization chamber (TIC) for fission fragment (FF) mass, kinetic energy and FF orientation. Correlated FF kinetic energies, their masses and the angle of the fission axes in 3D Cartesian coordinates can be determined from analysis of the heights and shapes of the pulses induced by the fission fragments on the anodes of TIC. Anodes of TIC were designed as consisting of isolated strips each having independent electronic circuitry and special multi-channel pulse processing apparatus. Mathematical algorithms were provided along with formulae derived for fission axis angles determination. It was shown how the point of fission fragments origin on the target plane may be determined using the same measured data. The last feature made the TIC a rather powerful tool for prompt fission neutron (PFN) emission investigation in event by event analysis of individual fission reactions from non point fissile source. Position sensitive neutron induced fission detector for neutron imaging applications with both thermal and low energy neutrons was found as another possible implementation of the designed TIC.

Keywords: **spontaneous fission, 252Cf, prompt fission neutron emission, neutron multiplicity, fission fragment mass distribution, total kinetic energy distribution.**
PACS: 24.75.+i; **25.85.Ca;** 28.20.-v; **29.40.Cs; 29.85.Fj.**

INTRODUCTION

A convenient way to study of PFN emission in spontaneous or neutron-induced fission is to use a traditional twin back-to-back ionization chamber, with two chambers sharing a common cathode [1]. The cathode is made from a thin conductive foil and at the same time serves as backing for the fissile deposit. For binary fission events the two complementary FF are simultaneously detected in two independent chambers. Free electrons released by FF deceleration are induced pulses on the chambers anodes and on the common cathode during drift along the applied externally electric field. The pulse height in each chamber was proportional to corresponding FF kinetic energy release and the FF pulse shape conveys information on the FF angle (Θ) in respect to the electric field applied in the direction of the normal to the cathode plane. From the correlated energies obtained in the above double-energy (2E) experiment, FF masses and velocities may be found [2]. If the point fissile target located on the common cathode's centre and the fast neutron detector (ND) was positioned at the certain distance along the normal to the target, then the angle between FF and the PFN emission would be equal to Θ. The PFN velocity may be determined from the known flight path and the measured time delay between cathode and ND pulses. Measured FF and PFN

velocity vectors then may be used to reconstruct the PFN emission kinematics. The PFN multiplicity distributions in respect to FF kinetic energy release and mass split may be reconstructed by comparison of two sets of FF measurements. In the first experiment fission fragment mass and kinetic energy release should be evaluated from the measurement independent from ND. In the second experiment FF mass and kinetic energy release should be evaluated for the FF coincided with ND. The obtained experimental results are of great demand for theoretical models of fission process development. The conventional chamber had limited suitability for investigations of nuclei with "zero thickness" or point sources like ^{252}Cf. The chamber of new design was developed mainly with intention to overcome that limitation and perform measurements with nuclei as ^{235}U, ^{239}Pu and other, which technically could not be made of point size, but they are important for new generation of nuclear energy production schemes.

Experimental Method

The detailed information on PFN emission in fission is available from the measured dependence of average number $\bar{\nu}(A,TKE)$ of PFN emitted by the FF with mass number A and TKE release of two fission fragments [1-3]. The late function allows obtaining of averaged characteristics on $\bar{\nu}(A)$ or $\bar{\nu}(TKE)$ by integrating over respective variable, if the mass yield matrix - *Y(A,TKE)* is known, for example:

$$\bar{\nu}(A)=\frac{\int_0^\infty \bar{\nu}(A,TKE)Y(A,TKE)dTKE}{\int_0^\infty Y(A,TKE)dTKE}, \qquad (1).$$

$$\bar{\nu}=\int_0^\infty \bar{\nu}(A,TKE)Y(A,TKE)dTKEdA, \quad 200=\int_0^\infty Y(A,TKE)dTKEdA$$

Similar relation could be written for averaging over A:

$$\bar{\nu}(TKE)=\frac{\int_0^\infty \bar{\nu}(A,TKE)Y(A,TKE)dA}{\int_0^\infty Y(A,TKE)dA}, \qquad (2).$$

$$\bar{\nu}=\int_0^\infty \bar{\nu}(A,TKE)Y(A,TKE)dTKEdA, \quad 200=\int_0^\infty Y(A,TKE)dTKEdA$$

Determination of $\nu(A),\nu(TKE)$ can be done if the measurement of $\nu(A,TKE)$ and $Y(A,TKE)$ could be arranged. For each fission event the FF and PFN kinetic energies, FF masses along with the angle between PFN and FF should be

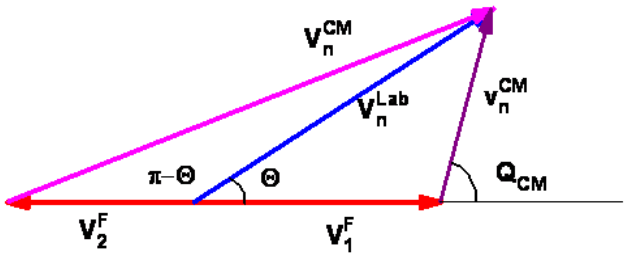

FIGURE 1. Vector diagram for PFN emission from FF.

determined in order to reconstruct the reaction kinematics and PFN emission from the individual FF in the centre of mass system (CM). Reaction kinematics is sketched in Fig. 1. The experimental setup consists of the position sensitive twin back-to-back ionization chamber (TIC), which was designated for FF kinetic energy release and the three cosines of angles between fission axis and the Cartesian axes.

Signal Formation on the Ionization Chamber anode

Signals from the TIC anodes arise because of the motion of charge carriers after they are formed by the FF. Once the last of the carriers arrives at its collecting electrode, the process of charge induction ends and the pulse is fully developed. The time evolution of the signal is of fundamental importance in understanding the timing properties of pulses as well as in predicting the effects of changes in the location of the radiation interactions on the shape of the pulse. The task of predicting the types of signals expected on a specific electrode segment also requires that a more basic approach be taken to predict induced charges. The Poisson equation is the starting point for these calculations. It can be written

$$\nabla^2\varphi = 0\text{, where } \nabla^2 = \frac{\partial^2}{\partial x^2} + \frac{\partial^2}{\partial y^2}\text{ - 2D Laplacian operator} \qquad (3)$$

For complex geometries or detector shapes, solutions can be obtained only numerically. The electric field at any point can be obtained simply by taking the gradient of the potential.

$$\varepsilon = -grad\varphi \qquad (4)$$

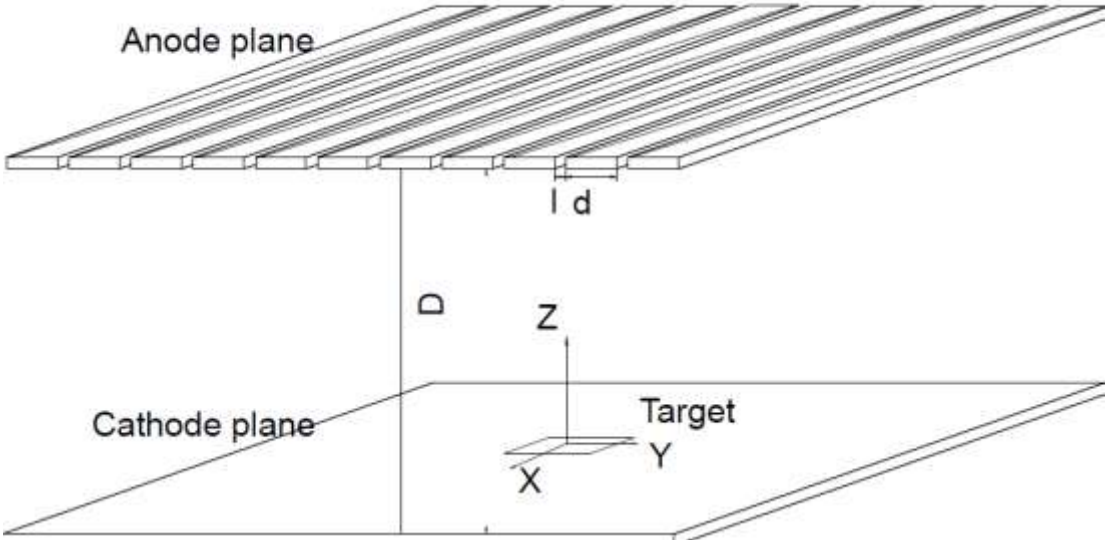

FIGURE 2. Sketch of the upper half of the twin back-to-back ionization chamber with strip anodes.

Neglecting the effects of diffusion, charge carriers generated within the detector will follow the electric field lines from their point of formation to the collecting electrode. If an

assumption is made about their velocity as a function of electric field (for example, a proportional relationship indicating a constant value of the mobility), then the position of the charge as a function of time can be uniquely determined. The general method to calculate induced charge on electrodes due to the motion of charge carriers in a detector makes use of the Ramo-Shockley Theorem [4] and the concepts of the **weighting field** and **weighting potential**. The theorem states that the instantaneous current induced on a given electrode is equal to $i = q\bar{v}E_0$ where q is the charge of the carrier, $\bar{v}$ is its velocity, and E_0 is called the weighting field. Another way of stating the same principle is that the induced charge on the electrode is given by the product of the charge on the carrier multiplied by the difference in the weighting potential ϕ_0 from the beginning to the end of the carrier path;

$$Q = q\Delta\varphi_0 \tag{5}$$

To find this weighting potential ϕ_0 as a function of position, one must solve the Laplace equation for the geometry of the detector, but with some artificial boundary conditions:

1. The voltage on the electrode for which the induced charge is to be calculated is set equal to unity.
2. The voltages on all other electrodes are set to zero.
3. Even if a trapped charge is present within the detector volume, it is ignored in the calculation.

The solution under these conditions gives the weighting potential, and its gradient is the weighting field. The weighting potential is not the actual electric potential in the detector, but instead serves as a convenience that allows simple determination of the induced charge on the electrode of interest by taking differences in the weighting potential at the start and end of the carrier motion. The path of the carrier must still be determined from the actual electric field. If the position of the carrier as a function of time is determined as previously described, then the time profile of the induced charge (or the induced current) can also be traced out to determine the shape of the output pulse.

Let us recall result of Ramo-Shokley theorem application to the Frisch-gridded ionization chamber [5]. When all FF decelerated inside cathode-grid area the charge *Q*, induced by whole electrons along a FF deceleration path, when they collected on the anode could be found as:

$$Q(E, D+s) = \int_0^L e \times \rho(\tau) \times (1 - \sigma \times \frac{\tau \times \cos(\Theta)}{D}) d\tau = N \times e \times (1 - \sigma \frac{\hat{X}(E) \times \cos(\Theta)}{D}) \tag{6}$$

In eq. 6 the $\hat{X}(E) = \int_0^L \tau \times \rho(E, \tau) d\tau$ is the "centre of charge" and $n(E) = \int_0^L \rho(E, x) dx$ is a total number of electrons, created during the FF deceleration, D – is the anode-grid, s – is the grid-anode distance and σ – is the grid inefficiency factor. Drift time ***T*** of the "charge centre" of FF ionization from the point of origin to the point with coordinate $y = D + \frac{s}{2}$ can be calculated as:

$$T(E, \cos(\Theta)) = \frac{D}{W}(1 + \frac{s}{2D} - \frac{\bar{X}(E)}{D}\cos(\Theta)) \tag{7}$$

Eq. 7 describes dependence of drift time *T* on *cos(Θ)*, where *Θ*-is the angle between fission axis and the cathode plane normal. The DPP algorithms and practical implementation of pulse height Q(D+s) and *T(cos(Θ))* were described in previous papers [7-9]. If the kinetic energy loss in target material (or target backing) can be neglected, then from Eq. 7 one can found the maximum and minimum drift time values are as follows:

$$T_{\max}(E) = \frac{D + 0.5 * s}{W}, \quad T_{\min}(E) = \frac{D + 0.5 * s + \bar{X}(Q)}{W} = T_{\max}(E) - \frac{\bar{X}(Q)}{W} \qquad (8)$$

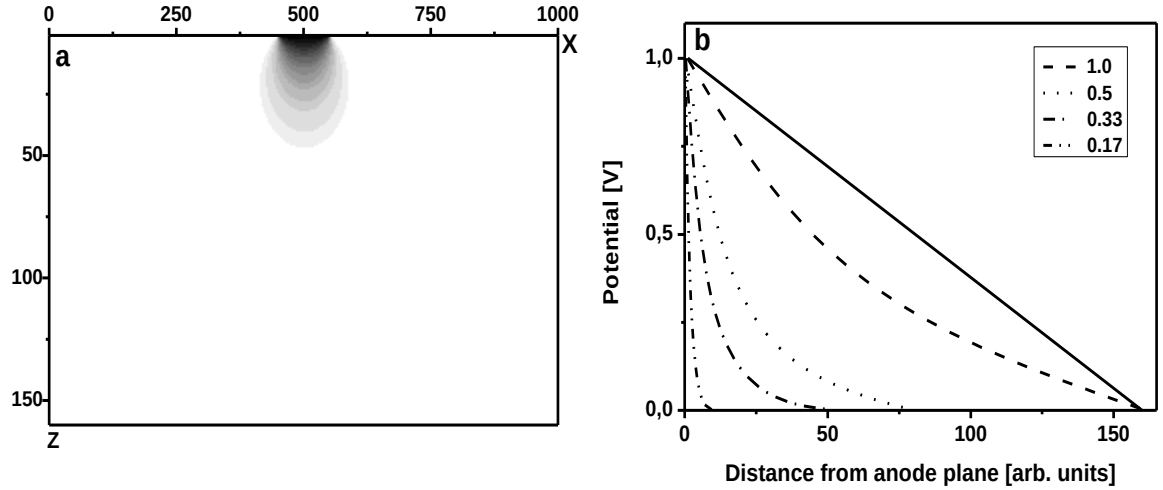

FIGURE 3. a) Weighting potential for single strip $\varphi_0(Z,Y)$. b) Dependence of weighting potential on distance for a given strip width to cathode-anode distance ratio

Let us consider position sensitive modification of a parallel plate ionization chamber sketched in Fig. 2. The *x-y* surface on the cathode plane is made of conventional continuous electrode. The anode surface consists of the thin cooper foil, subdivided into the Δ-electrodes. Each Δ-electrode is an independent triangle electrode, and small gaps are present between adjacent parts. Separate electrical contacts generally are made to each Δ-electrode. We assume that no fixed charges (space charge) are present in the detector volume. For simplicity, we also assume that the dimensions of the detector in the *x* and y directions are large compared with the anode-cathode distance, so that edge effects can be neglected in the following analysis. If the same positive potential is applied to all Δ-electrodes then the solution of Laplace equation at the distances much greater than the gap width is equivalent to the case in which a single continuous electrode was to replace the Δ-pattern. The potential changes linearly between the anode-cathode area, and the electric field is essentially uniform throughout the volume. If the Δ-electrodes are operated at a positive potential relative to the opposite surface, then electrons will be attracted along field lines that are parallel to each other and perpendicular to the anode surfaces. Neglecting diffusion, they will be collected by the Δ-electrode that lies directly to the up of the point at which the charges are formed within the volume. The positive ions move in the opposite direction and toward the continuous cathode at the bottom surface of the detector. In order to predict the electrical signal expected from a typical single Δ-electrode, we must apply the Shockley-Ramo theorem to this case to first find the configuration of the weighting potential. We again solve the same Laplace equation, but now with

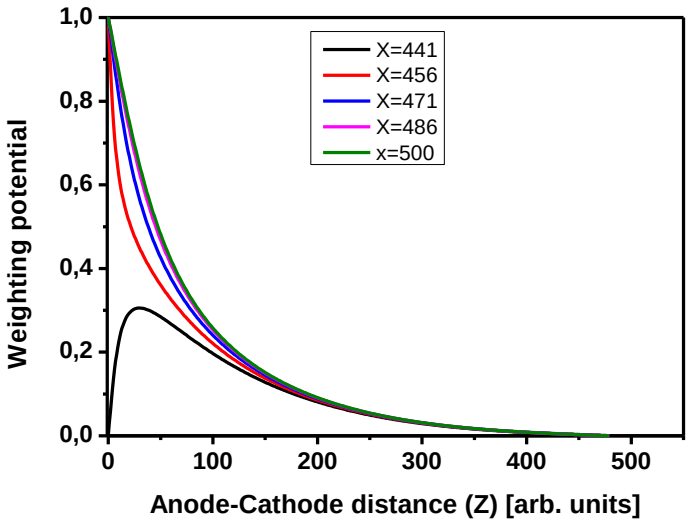

FIGURE 4. Dependence of weighting potential φ_0(X=const,Z) on distance from the selected strip.

boundary conditions that set the potential of the strip of interest to 1 V, and the potential of all other strips and the cathode on the opposite surface to zero. The typical solution is presented in fig. 3a. Dependence of weighting potential from the cathode-anode distance is presented on fig. 3b for various values of the ratio of strip width to cathode-anode distance. If the ratio is sufficiently small then the strip signal rise follows the potential grown and happens in this case in close proximity of the strip. Thank to that there is no angle dependence on the strip signal like in Frisch-gridded ionization chamber. Neglecting diffusion the electric charge induced on the strip by ionization charge can be calculated using Eq. 5. From analysis of weighting potential dependence on the distance from the strip (see Fig. 4) one could conclude that all charges collected on the selected strip will induce nonzero charge, but the charges collected on the adjacent strips do not induce charge at all.

Our goal was to determine the (x,y) coordinate of the point where charge was collected on the strip from analysis of the signals on Δ- electrodes composing the strip. The sum of these two signals can be calculated as a signal from the undivided strip. It is reasonable to assume that the difference between these signals was proportional to the shift (positive or negative) of charge position from the strip centre. Let the origin of Cartesian coordinate system is located in the centre of square cathode (see fig. 10) and each Δ-electrode has individual charge integrating preamplifier. Then the sum and difference of output signals from the individual strips can be interpreted as measure of (x,y) coordinate of the charge distribution centre from the electrons collected by the considered strip. Similarly the z-coordinate of the charge distribution can be evaluated as electron drift velocity product with the time difference between the strips and cathode signal. When all detected strip signals are recorded along with their drift times then the set of samples along the FF range was available. Two correlated FF detection by back-to-back twin ionization chamber was assumed in fig. 10. For each fission event the following information can be determined:

$$\frac{x_1 - x_0}{x_1 + x_2} = \frac{R_1}{R_1 + R_2} \Rightarrow x' = x_1 - x_0 = (x_1 + x_2)\frac{R_1}{R_1 + R_2} \qquad \frac{x_2 + x_0}{x_1 + x_2} = \frac{R_2}{R_1 + R_2} \Rightarrow x' = x_2 + x_0 = (x_1 + x_2)\frac{R_2}{R_1 + R_2}$$

$$\frac{y_1 - y_0}{y_1 + y_2} = \frac{R_1}{R_1 + R_2} \Rightarrow y' = y_1 - y_0 = (y_1 + y_2)\frac{R_1}{R_1 + R_2} \qquad \frac{y_2 + y_0}{y_1 + y_2} = \frac{R_2}{R_1 + R_2} \Rightarrow y' = y_2 + y_0 = (y_1 + y_2)\frac{R_2}{R_1 + R_2}$$

$$COS(X) = \frac{x_1 + x_2}{R_1 + R_2};\ \mathrm{COS(X)} = \frac{x_2 + x_0}{R_2};\mathrm{COS(Y)} = \frac{y_1 + y_2}{R_1 + R_2};\ \mathrm{COS(Y)} = \frac{y_2 + y_0}{R_2};COS(Z) = \frac{z_1}{R_1};\ COS(Z) = -\frac{z_2}{R_2}$$

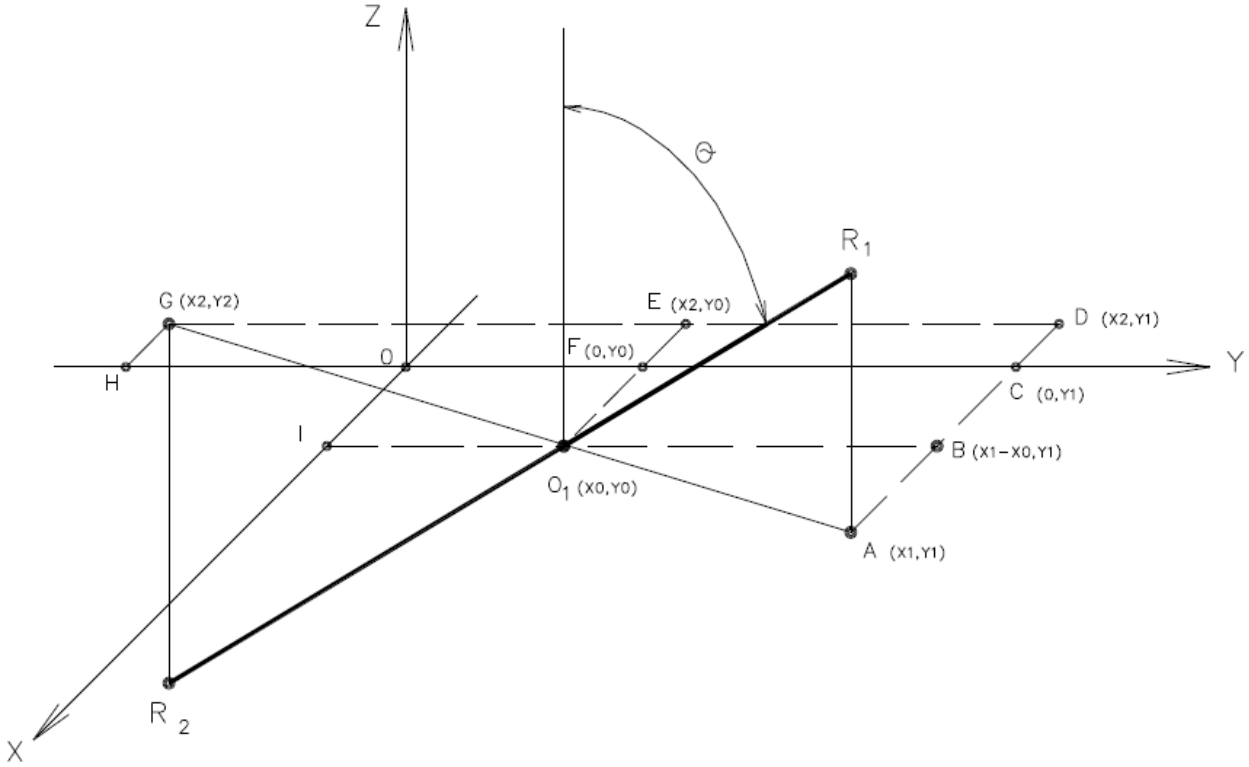

FIGURE 5. Evaluation of fission axis coordinates and determination of FF point of origin coordinates.

Where (x_0,y_0) is the coordinates of FF point of origin, (x_1,y_1) is the coordinate of the FF range in the upper chamber (positive direction of Z-axis); (x_2,y_2) is the coordinate of the correlated FF range in the lower chamber; (z_1,z_2) is the are z-coordinates of the FFs range in upper and lower chambers respectively. The Y-coordinates can be evaluated from the sum signals taken from two Δ-electrodes, the X-coordinates may be evaluated from the difference of signals and Z-coordinates may be evaluated from the measured drift time.

Conclusions

We presented recent achievements in development of new fission detector and advanced mathematical data analysis, which we believe opens a new perspective in study of PFN emission in low energy fission. With new chamber design the fission axis coordinates measurement became possible for non point fissile targets. A new detector can be used in neutron imaging applications due to availability of FF point of origin coordinates with pretty good precision. It is well known that neutron imaging application requires very good spatial resolution (<0.1 mm) so far achieved using CCD camera. According to our estimate using the mathematical model presented above the spatial resolution in case of PFN emission can be about ~0.5 mm with strip width of 5 mm. For neutron imaging application apparently strip width can be made narrower.

REFERENCES

1. C. Budtz-Jørgensen and H.-H. Knitter, *Nucl. Phys.*, A490, 307 (1988).
2. C. Wagemans, The Nuclear Fission Process, Boca Raton: Boca Raton, 1991.
3. Sh. Zeynalov, O.V. Zeynalova, F.-J. Hambsch, S. Oberstedt, Physics Procedia Volume 31, 2012, pp 132–140
4. G.F. Knoll, Radiation detection and measurements, New York: Wiley, 2000.
5. O. Zeynalova, Sh. Zeynalov, M. Nazarenko, F.J. Hambsch, and S. Oberstedt, AIP Conf. Proc. 1404, 325 (2011).
6. O. Zeynalova, Sh. Zeynalov, F.-J. Hambsch and S. Oberstedt, "DSP Algorithms for Fission Fragment and Prompt Fission Neutron Spectroscopy in *Application of Mathematics in Technical and Natural Sciences-2010*, edited by M. D. Todorov and C. I. Christov, AIP Conference Proceedings 1301, American Institute of Physics, Melville, NY, 2010, pp. 430-439.
7. O.V. Zeynalova, Sh. S. Zeynalov, F.-J. Hambsch, S. Oberstedt, *Bulletin of Russian Academy of Science: Physics*, 73, 506-514 (2009).